



Assessment of finite difference models for water content determination in soils of the semi-arid region of Brazil

Daniel Milian Pérez^a, Abel Gámez Rodríguez^a, Yaicel Ge Proenza^a, Frederico Dias Nunes^a, Antonio Celso Dantas Antonino^a, José Romualdo de Sousa Lima^b, Severino Martins dos Santos Neto^c, Artur Paiva Coutinho^c, Marcus Metri Correa^d

^a Universidade Federal de Pernambuco-UFPE. Av. Professor Luiz Freire, n. 1000, Cidade Universitária, Recife, Pernambuco, Brasil. CEP: 50.740-545. E-mail: daniel.milian@ufpe.br, abel.rodriguez@ufpe.br, yaicel.geproenza@ufpe.br, frederico.nunes@ufpe.br, antonio.antonino@ufpe.br.

^b Universidade Federal do Agreste de Pernambuco-UFAPE. Av. Bom Pastor, s/n, Garanhuns, Pernambuco, Brasil. CEP: 55.292-278. E-mail: romualdo.lima@ufrpe.br.

^c UFPE, Centro Acadêmico do Agreste-CAA. Av. Marielle Franco, s/n, km 59, Nova Caruaru, Caruaru, Pernambuco, Brasil. CEP: 55.014-900. E-mail: severino.martins@ufpe.br, arthur.coutinho@ufpe.br.

^d Universidade Federal Rural de Pernambuco-UFRPE, Departamento de Tecnologia Rural. Rua Dom Manoel de Medeiros, s/n, Dois Irmãos, Recife, Pernambuco, Brasil. CEP: 55.292-278. E-mail: marcus.mcorrea@ufrpe.br.

ARTICLE INFO

Received 28 Sep 2024

Accepted 04 Dec 2024

Published 13 Dec 2024

ABSTRACT

The water content in soil and its variation with depth are critical for numerous processes, significantly influencing plant growth, soil mechanics, and physical and chemical properties. In the semi-arid region of northeastern Brazil, where the Caatinga biome is located, accurate estimation of soil water content is crucial due to severe water scarcity and highly variable precipitation patterns. This study aimed to evaluate the sensitivity and accuracy of a computational model for predicting soil matric potential and water content. The model solves the Richards' equation using three finite difference methods: explicit, implicit, and Crank-Nicolson. The methods were applied to three soil textures (sandy loam, silt, and clay), and a preliminary analysis was performed to identify the optimal time (dt) and spatial (dz) steps for achieving relative differences below 1%. The model predicted acceptable soil matric potential and water content behavior, particularly for sandy loam, which required finer steps (1 second, 1 cm) compared to silt and clay (10 seconds, 5 cm). Two test cases from the literature were used for further validation. Finally, the model was applied to soil textures typical of northeastern Brazil, confirming its ability to capture the dynamics of soil water content in this region. The results highlight the applicability of this computational approach to semi-arid soils, contributing to improved water management and crop production strategies.

Keywords: Matric potential, soil water content, finite differences, explicit method, implicit method, semi-arid.



Journal of Environmental Analysis and Progress © 2016
is licensed under CC BY-NC-SA 4.0

Introduction

The widespread effects of climate change threaten both natural and human ecosystems. Although the extent of these effects is different worldwide, all continents are positively or negatively impacted (Assouline et al., 2024). Water resources, vital to maintaining any ecosystem's health and proper functioning, have been identified as especially vulnerable to global climate change (Shukla et al., 2019; Althoff et al., 2021). Additionally, meteorological variables, such as temperature and precipitation, considerably impact water resources (Sishodia et al., 2017; Daneshi et

al., 2020). These effects might represent even greater implications for the semi-arid region in the northeastern part of Brazil, in which the Caatinga biome is located. This biome has specific climatic conditions, mainly high temperatures, and severe water scarcity because it relies on a fluctuating and drought-precipitation pattern (Shukla et al., 2019; Brito et al., 2020).

The Caatinga biome covers approximately 1 million km² of the Northeast area of Brazil. This region has scarce precipitations throughout the year (below 1000 mm a year), and the rain distribution is far from uniform. In fact, 20% of the annual

precipitation occurs in one day, and up to 60% can be observed over a month. In addition, the average temperatures in the Caatinga biome are high (up to 27°C), with less than 50% relative humidity throughout the year. These favorable conditions for evapotranspiration processes result in water shortages for most of the year (PBMC, 2014). Compounding this scenario, studies carried out by the Brazilian Panel on Climate Change indicate that by 2040, that area may experience an increase in the average air temperatures (up to 1°C) and a reduction within 10-20% in rainfall (PBMC, 2014; Brito et al., 2020). The expected increase in temperature and decrease in precipitation levels threaten to make the region even more arid (Cirilo, 2008). Vieira et al. (2015) reinforced these conclusions, which reported that 94% of the northeast Brazilian drylands were susceptible to desertification (Vieira et al., 2015). The degradation of these areas may cause harmful effects not only to their inhabitants, crops, and livestock productivity but also to the native species. It was estimated that up to 28 native species are in danger of extinction due to the degradation of the Caatinga biome and its neighboring areas (LEAL et al., 2005; PBMC, 2014; Shukla et al., 2019).

Therefore, the effects of global climate change in the Caatinga biome must be effectively evaluated to set up a sustainable scheme for managing water resources. To address this concern, a complete characterization of the parameters and properties of the soil from the Caatinga biome is increasingly necessary. The soil water content is one variable that allows this evaluation to be carried out (Rad et al., 2017). The water content in the soil, although representing just a small part of the worldwide water resources, plays a key role in the functioning of ecosystems (Liu et al., 2024). It affects several soil's mechanical, physical, and chemical properties and greatly impacts plant growth and productivity. The soil water content is directly related to the soil water potential. This potential is variably related to time and space. It depends on the water balance within the soil, which is an equilibrium condition between the water inlet (rain, irrigation) and outlet (drainage, evaporation, and root absorption) routes (Hillel, 1998; Chavarria & dos Santos, 2012).

This study aimed to evaluate the sensitivity and accuracy of a mathematical model for estimating the soil matric potential and water content.

Material and Methods

The proposed model in this study solves Richards' equation using finite differences using three methods: explicit, simple implicit, and the

Crank-Nicolson approach. Although these numerical methods are well-established and commonly used in soil science, their application to the unique conditions of semi-arid soils, such as those found in the northeastern region of Brazil, represents a novel contribution. This region, characterized by extreme water scarcity and highly variable rainfall patterns, presents significant challenges for soil moisture prediction. To address this, a preliminary sensitivity analysis was carried out to determine the optimal range of variation of the time and spatial steps and the influence of these steps on the results. Three soil textures (sandy loam, silt, and clay), six discrete spatial steps (0.5, 1, 2, 4, 5, and 10 cm), and five discrete steps (0.1, 1, 10, 100, and 1000 seconds) were considered. Once the proper parameters were identified, the proposed computational model was used to calculate the soil matric potential and water content of twelve soil textures. With the estimated sensitivity as starting data, two test cases available in the literature were solved. Finally, the influence of the numerical solution method in soils of the semi-arid region of Brazil was studied, using experimental material composition data of the soil from two locations in the northeastern part of Brazil, particularly in the municipality of São Bento do Una in the state of Pernambuco.

The water flow through unsaturated porous media is usually described using the Richards' equation (Richards, 1931). A prevalent formulation of Richards' equation for unidirectional problems is the combination of the Darcy equation (Equation 1), the continuity equation (Equation 2), and the soil-specific hydraulic capacity (C) equation (Equation 3), assuming the reference system to be on the ground surface (Farthing & Ogden, 2017).

$$q = -K(h) \cdot \left(\frac{dh}{dz} - 1 \right) \quad \text{Eq. (1)}$$

$$\frac{d\theta}{dt} = -\frac{dq}{dz} \quad \text{Eq. (2)}$$

$$C(h) = \frac{d\theta}{dh} \quad \text{Eq. (3)}$$

where q is the flow rate through the perpendicular unit area; h is the matric potential; K is the empirical unsaturated hydraulic conductivity (a proportionality factor related to porosity and viscosity); θ is the volumetric soil moisture given as the volume of water per gram of dry medium; z is the vertical coordinate; and t is the time (Hillel, 1998). Considering a function only of the matric potential and the independent parameters (time and coordinate), Equation 4 can be expressed.

$$C(h) \cdot \frac{dh}{dt} = \frac{d}{dz} \left(K(h) \cdot \left(\frac{dh}{dz} - 1 \right) \right) \quad \text{Eq. (4)}$$

Although Richards' equation has long been used for simulation purposes, analytical solutions, such as those provided by the Gardner model (Zhu et al., 2019; Wu et al., 2024), are limited to idealized or simplified systems. For real-life or complex systems, especially those involving heterogeneous soils or variable boundary conditions, obtaining analytical solutions is challenging, and numerical methods are often required. While these numerical solutions can be computationally expensive (Farthing & Ogden, 2017), they remain essential due to the complexity of real-world scenarios, where analytical solutions are generally not applicable. In addition to the Richards' equation, the Mualem–van Genuchten equations (Equations 5-7), proposed by Mualem in 1976 and modified by van Genuchten four years later (Mualem, 1976; van Genuchten, 1980), are preferred.

$$K(h) = K_s \cdot \frac{(1-(\alpha|h|)^{n-1} \cdot (1+(\alpha|h|)^n)^{-m})^2}{(1+(\alpha|h|)^n)^{0.5 \cdot m}} \quad \text{Eq. (5)}$$

$$C(h) = \frac{m \cdot n \cdot \alpha^n \cdot (\theta_s - \theta_r) \cdot |h|^{n-1}}{(1+(\alpha|h|)^n)^{m+1}} \quad \text{Eq. (6)}$$

$$\theta(h) = \frac{(\theta_s - \theta_r)}{(1+(\alpha|h|)^n)^m} + \theta_r \quad \text{Eq. (7)}$$

where K_s is the saturated hydraulic conductivity; α , m , n are parameters which depend on the type of soil; and θ_s and θ_r are the volumetric moisture of the saturated soil and the residual volumetric moisture of the soil, respectively (Mualem, 1976; van Genuchten, 1980; Hillel, 1998).

Richards' equation is a markedly nonlinear degenerate elliptic-parabolic partial differential equation. Under these conditions, obtaining a solution using traditional analytical techniques is very difficult. Furthermore, the nonlinearity and the degeneracy make it difficult to use numerical methods (Farthing & Ogden, 2017). Thus, discretizing the derivative operators is almost a general rule for solving the equation numerically for water infiltration simulations. A conventional approach uses the finite difference method with constant discrete time and spatial steps, dt and dz , respectively. Several schemes (explicit, simple implicit, and Crank-Nicolson) can be used to obtain the numerical solution of these equations (Hillel, 1998; Schneider, 2003; Bittelli et al., 2015; Pedrozo et al., 2015), which are described in the following sections. Although more advanced numerical methods, such as preconditioned iterative methods, multigrid techniques, and global

correction methods, have been developed to improve the convergence rate and computational efficiency of nonlinear processes (Lott et al., 2012; Arioli & Scott, 2014; List & Radu, 2016), the current study prioritizes the use of simpler finite difference approaches. These methods were chosen to establish a baseline for applying Richards' equation to the specific conditions of the semi-arid region of northeastern Brazil. Future work could explore integrating more advanced techniques to optimize the simulation process further.

Explicit method

The differential equation is numerically solved in the explicit finite difference scheme by approximating the temporal derivative using a forward finite difference at time t^n and a second-order central difference for the spatial derivative at position z_i . Applying these approximations to Equation 4, the finite difference mode of the Richards' equation can be written as Equation 8. The Equation 9 is used to calculate the matric potential value at the next time t^{n+1} using the previous value in the z_{i-1} , z_i and z_{i+1} points. The interblock hydraulic conductivity values $K(h_{i\pm 0.5}^n)$ may be calculated by the arithmetic, geometric or harmonic mean (Vasconcellos & Amorin, 2001); however, the integral mean (Equation 10), as suggested by Pedrozo et al. (2015), was used with the explicit algorithm (Pedrozo et al., 2015; Pedrozo et al., 2016). Nevertheless, note that the hydraulic conductivity and the specific hydraulic capacity values are updated after every iteration while propagating the Equation 9 because they are h -dependent.

$$C(h_i^n) \frac{h_i^{n+1} - h_i^n}{\Delta t} = \frac{1}{\Delta z} \left[K(h_{i+0.5}^n) \left(\frac{h_{i+1}^n - h_i^n}{\Delta z} - 1 \right) - K(h_{i-0.5}^n) \left(\frac{h_i^n - h_{i-1}^n}{\Delta z} - 1 \right) \right] \quad \text{Eq. (8)}$$

$$h_i^{n+1} = h_i^n + \frac{\Delta t}{C(h_i^n) \Delta z} \left[K(h_{i+0.5}^n) \left(\frac{h_{i+1}^n - h_i^n}{\Delta z} - 1 \right) - K(h_{i-0.5}^n) \left(\frac{h_i^n - h_{i-1}^n}{\Delta z} - 1 \right) \right] \quad \text{Eq. (9)}$$

$$K(h_{i+0.5}^n) = \frac{1}{h_{i+1}^n - h_i^n} \int_{h_i^n}^{h_{i+1}^n} K(h) dh \quad \text{Eq. (10)}$$

Simple implicit method

Implicit methods are commonly used to circumvent the stability restriction of explicit methods. The simple implicit method approximates the temporal derivative using a backward, a finite difference at time t^{n+1} , and a second-order central difference for the spatial derivative at position z_i (Schneider, 2003). Equation 4 is then represented by the simple

implicit method (Equation 11). Applying Equation 12 with the coefficients (13 to 16) to the internal nodes (from z_2 to z_{n-1}), results in a tridiagonal system of equations, which is resolved by the Thomas' algorithm (Chapra & Canale, 2015). To solve the system 12-16, it is necessary to implement a predictor/corrector algorithm, since the $K(h_{i\pm 0.5}^{n+1})$ and $C(h_i^{n+1})$ values are missed.

$$C(h_i^{n+1}) \frac{h_i^{n+1} - h_i^n}{\Delta t} = \frac{1}{\Delta z} \left[K(h_{i+0.5}^{n+1}) \left(\frac{h_{i+1}^{n+1} - h_i^{n+1}}{\Delta z} - 1 \right) - K(h_{i-0.5}^{n+1}) \left(\frac{h_i^{n+1} - h_{i-1}^{n+1}}{\Delta z} - 1 \right) \right] \quad \text{Eq. (11)}$$

$$e_i h_{i-1}^{n+1} + f_i h_i^{n+1} + g_i h_{i+1}^{n+1} = b_i \quad \text{Eq. (12)}$$

$$e_i = \frac{K(h_{i-0.5}^{n+1})}{\Delta z^2} \quad \text{Eq. (13)}$$

$$f_i = - \left(\frac{C(h_i^{n+1})}{\Delta t} + \frac{K(h_{i+0.5}^{n+1}) + K(h_{i-0.5}^{n+1})}{\Delta z^2} \right) \quad \text{Eq. (14)}$$

$$g_i = \frac{K(h_{i+0.5}^{n+1})}{\Delta z^2} \quad \text{Eq. (15)}$$

$$b_i = \frac{K(h_{i+0.5}^{n+1}) - K(h_{i-0.5}^{n+1})}{\Delta z} - \frac{C(h_i^{n+1}) h_i^n}{\Delta t} \quad \text{Eq. (16)}$$

Then, an initial estimation of h_i^{n+1} is obtained by resolving the system with the $K(h_{i\pm 0.5}^n)$ and $C(h_i^n)$ values, and the system is subsequently solved using this previous evaluation. In consequence, the system must be solved twice in each time step. The geometric mean (Equation 17 is for $K(h_{i\pm 0.5}^{n+1})$) was used for estimating the interblock K values.

$$K(h_{i\pm 0.5}^{n+1}) = \sqrt{K(h_i^{n+1}) \cdot K(h_{i\pm 1}^{n+1})} \quad \text{Eq. (17)}$$

Crank-Nicolson method

A recommended approach is the implicit Crank-Nicolson finite difference scheme, which is second-order accurate in space and time. It can be implemented by approximating the temporal derivative using a central finite difference at time $t^{n+1/2}$, and a second-order central difference for the spatial derivative at position z_i . The spatial difference at time $t^{n+1/2}$ is obtained as the mean of the spatial differences evaluated at t^n and t^{n+1} . Therefore, the Richards' equation in mode of finite differences by Crank-Nicolson is as follows (Equations 18-23):

$$C(h_i^{n+0.5}) \frac{h_i^{n+1} - h_i^n}{\Delta t} = \frac{0.5}{\Delta z} \left[K(h_{i+0.5}^n) \left(\frac{h_{i+1}^n - h_i^n}{\Delta z} - 1 \right) - K(h_{i-0.5}^n) \left(\frac{h_i^n - h_{i-1}^n}{\Delta z} - 1 \right) + \right. \quad \text{Eq. (18)}$$

$$\left. K(h_{i-0.5}^{n+1}) \left(\frac{h_i^{n+1} - h_{i-1}^{n+1}}{\Delta z} - 1 \right) \right] \quad \text{Eq. (18)}$$

$$e_i h_{i-1}^{n+1} + f_i h_i^{n+1} + g_i h_{i+1}^{n+1} = b_i \quad \text{Eq. (19)}$$

$$e_i = \frac{0.5 \cdot K(h_{i-0.5}^{n+1})}{\Delta z^2} \quad \text{Eq. (20)}$$

$$f_i = - \left(\frac{C(h_i^{n+0.5})}{\Delta t} + \frac{K(h_{i+0.5}^{n+1}) + K(h_{i-0.5}^{n+1})}{2\Delta z^2} \right) \quad \text{Eq. (21)}$$

$$g_i = \frac{0.5 \cdot K(h_{i+0.5}^{n+1})}{\Delta z^2} \quad \text{Eq. (22)}$$

$$b_i = \frac{K(h_{i+0.5}^{n+1}) - K(h_{i-0.5}^{n+1})}{\Delta z} - \frac{C(h_i^{n+0.5}) h_i^n}{\Delta t} - \frac{0.5}{\Delta z} \left[K(h_{i+0.5}^n) \left(\frac{h_{i+1}^n - h_i^n}{\Delta z} - 1 \right) - K(h_{i-0.5}^n) \left(\frac{h_i^n - h_{i-1}^n}{\Delta z} - 1 \right) \right] \quad \text{Eq. (23)}$$

As in the simple implicit method, a tridiagonal system of equations is solved twice for each time step. The $C(h_i^{n+0.5})$ values in the corrector step are calculated as the mean value between the $C(h_i^n)$ value and that obtained by the predictor step. The geometric mean was used for estimating the interblock K values.

Soil characterization and properties

As previously explained, three groups of simulations were carried out. In the first group of simulations, twelve soil textures proposed by (Carsel & Parrish, 1988) were studied. The second study solved two test tasks proposed by (Celia et al., 1990) and (Miranda et al., 2005; Wendland & Pizarro, 2010). Finally, soils of the semi-arid region of northeast Brazil were studied.

Tables 1 and 2 summarize the values of the Van Genuchten parameters used to simulate the twelve soil textures and the two test cases. The Van Genuchten parameters used for simulating the soils of the semi-arid region of Brazil are shown in Table 3, including the hydrodynamic characterization of two soils of the municipality of São Bento do Una, in the Pernambuco state, reported in (Soares et al., 2020). The first of these soil plots consists of 2.0 ha of natural soil, where the Caatinga vegetation is preexistent, and the second consists of 4.5 ha of soil cultivated with forage palm (Soares et al., 2020). It was reported that a semi-arid climate predominates in that region, with a hot and dry summer and a rainy period extending from April to June (Soares et al., 2020).

Table 1. Van Genuchten parameters of the twelve soil textures, including the three soil textures used for the sensitivity analysis. Font: Carsel & Parrish (1988).

Soil texture	θ_r	θ_s	α (m ⁻¹)	n	K_s (m s ⁻¹)
Sand	0.045	0.43	14.5	2.68	8.243·10 ⁻⁵
Loamy sand	0.057	0.41	12.4	2.28	4.053·10 ⁻⁵
Sandy loam	0.065	0.41	7.5	1.89	1.228·10 ⁻⁵
Loam	0.078	0.43	3.6	1.56	2.889·10 ⁻⁶
Silt	0.034	0.46	1.6	1.37	6.944·10 ⁻⁷
Silt loam	0.067	0.45	2.0	1.41	1.250·10 ⁻⁶
Sandy clay loam	0.100	0.39	5.9	1.48	3.639·10 ⁻⁶
Clay loam	0.095	0.41	1.9	1.31	7.222·10 ⁻⁷
Silty clay loam	0.089	0.43	1.0	1.23	1.944·10 ⁻⁷
Sandy clay	0.100	0.38	2.7	1.23	3.333·10 ⁻⁷
Silty clay	0.070	0.36	0.5	1.09	5.556·10 ⁻⁸
Clay	0.068	0.38	0.8	1.09	5.556·10 ⁻⁷

Table 2. Van Genuchten parameters for the two test cases. Font: Celia et al. (1990), Miranda et al. (2005), Wendland & Pizarro (2010).

Test case	θ_r	θ_s	α (m ⁻¹)	n	K_s (m s ⁻¹)	Reference
1	0.102	0.368	3.35	2.0000	9.220·10 ⁻⁵	Celia et al., (1990)
2	0.000	0.443	4.49	3.6732	1.515·10 ⁻⁵	Miranda et al., (2005) Wendland & Pizarro, (2010)

Table 3. Van Genuchten parameters for the soils of the semi-arid region of Brazil. Font: Soares et al. (2020).

Study case	θ_r	θ_s	α (m ⁻¹)	n	K_s (m s ⁻¹)
Natural	0.033	0.344	3.29	2.64	5.380·10 ⁻⁶
Cultivated	0.065	0.437	6.22	2.95	1.780·10 ⁻⁵

Boundary and initial conditions, discretization, and model implementation

All simulations were carried out considering initial and boundary conditions of the

Dirichlet type with a known pressure head. Table 4 shows the boundary and initial conditions used in the simulations of the two test cases and the soils of the semi-arid region of the northeast of Brazil.

Table 4. Boundary and initial conditions used in the calculations, where the h and L values are in meters and t in hours. Font: Celia et al. (1990), Miranda et al. (2005), Wendland & Pizarro (2010).

Case	$h(z, 0)$	$h(L, t)$	$h(0, t)$	L	t	Reference
Test case 1	-10.00	-10.00	-0.75	1.00	24.00	(Celia et al., 1990)
Test case 2	-0.686524	-0.686524	-0.062476	0.70	1.75	(Miranda et al., 2005; Wendland & Pizarro, 2010)
Semi-arid	-0.42	-0.42	-0.04	0.50	2.00	-

The sensitivity analysis and the simulations of the twelve soil textures were performed considering a homogeneous initial head distribution and lower boundary condition of -1 m, the upper boundary condition is fixed at $h = -0.1$ m, the soil column was assumed to be 1 m deep, and the simulation time was 24 hours. Considering the initial sensitivity study with three soil textures (sandy loam, silt, and clay), six discrete spatial steps (0.5, 1, 2, 4, 5, and 10 cm) and five discrete steps (0.1, 1, 10, 100, and 1000 seconds) were analyzed. The results of this initial sensitivity study allowed us to define the parameters dt and dz for the subsequent calculations. Python 3.0 code was used to implement the proposed computational

model. The simulations were conducted on a personal computer with an Intel(R) Core(TM) i7-2600 CPU @ 3.40GHz and 16 GB of RAM.

Results and Discussion

As a first step, a sensitivity analysis for the dt and dz parameters was performed to define the best combination of values to guarantee the independence of the discretization results assumed for a range of soil textures. Three soil textures (sandy loam, silt, and clay), six discrete spatial steps (0.5, 1, 2, 4, 5, and 10 cm), and five discrete time steps (0.1, 1, 10, 100, and 1000 seconds) were studied. It was assumed that the simulation results are independent of the discretization scheme used

when the relative differences between the current and the previous step are less than 1%. The first parameter analyzed was dz , assuming a constant value of dt equals 1 second. Table 5 shows the maximum relative differences in the calculated soil water contents for the three soil textures and six discrete spatial steps studied. As observed in Table 5, the Sandy loam was the soil texture with the highest computational requirements (requires the smallest spatial discretization) to obtain an appropriate independence of the results from the

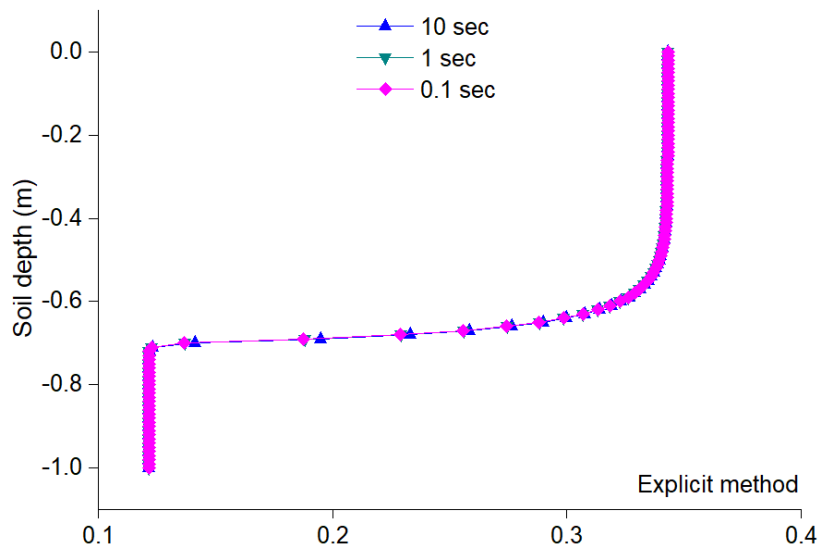
spatial discretization (dz). A relative difference of less than 1% was only obtained for a spatial discretization of 1.0 cm. The Silt soil texture requires a dz of 5 cm, while the Clay soil texture achieves relative differences below 1% even for a dz of 10 cm. This study indicated that at least 1.0 cm at the length of spatial discretization is compulsory to obtain water content values independent of the analyzed parameters for all analyzed soil textures. These results resulted in subsequent calculations with $dz = 1$ cm.

Table 5. Maximum relative differences (%) for the three soil textures (sandy loam, silt, clay) and six spatial steps ($dz = 10, 5, 4, 2,$ and 1 cm) after 24 hours. Font: Pérez et al. (2024).

Soil texture	Explicit method				
	10 cm	5 cm	4 cm	2 cm	1 cm
Sandy loam	10.5	3.2	1.6	1.4	0.5
Silt	1.2	0.3	< 0.0	< 0.0	< 0.0
Clay	< 0.1	< 0.1	< 0.0	< 0.0	< 0.0
Simple Implicit method					
Sandy loam	59.5	5.3	3.7	1.9	0.7
Silt	1.7	0.4	0.1	0.1	< 0.0
Clay	< 0.1	< 0.0	< 0.0	< 0.0	< 0.0
Crank-Nicolson method					
Sandy loam	59.5	5.6	4.0	2.1	0.9
Silt	1.7	0.4	0.1	0.1	< 0.0
Clay	< 0.1	< 0.0	< 0.0	< 0.0	< 0.0

The next step was the sensitivity analysis of the time discretization (dt). Figures 1, 2, and 3 show the soil water content profile distribution with depth for the three soil textures analyzed with

the corresponding discrete time steps: 0.1, 1, 10, 100, and 1000 seconds for the three calculation methods. The results with the explicit method for 100 and 1000 seconds are not included due to its instability with high values of dt .



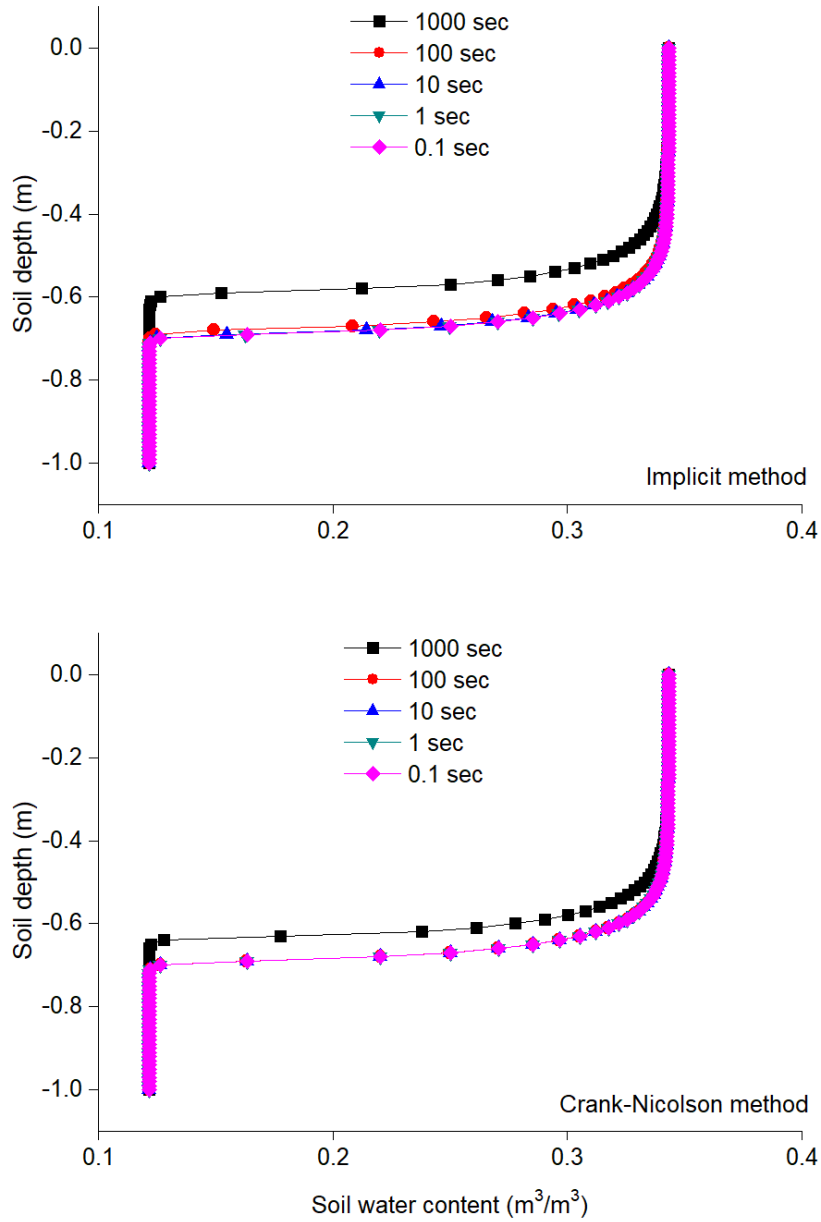
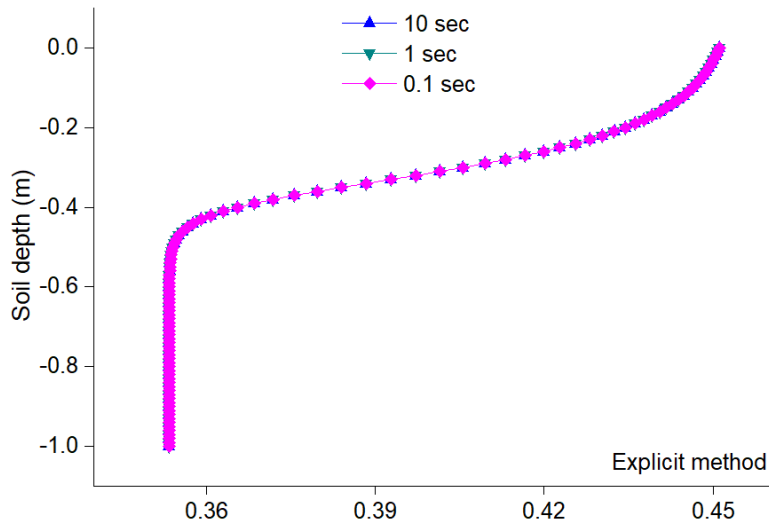


Figure 1. Soil water content obtained from simulations of the soil texture of Sandy loam ($t = 24$ h). Font: Pérez et al. (2024).



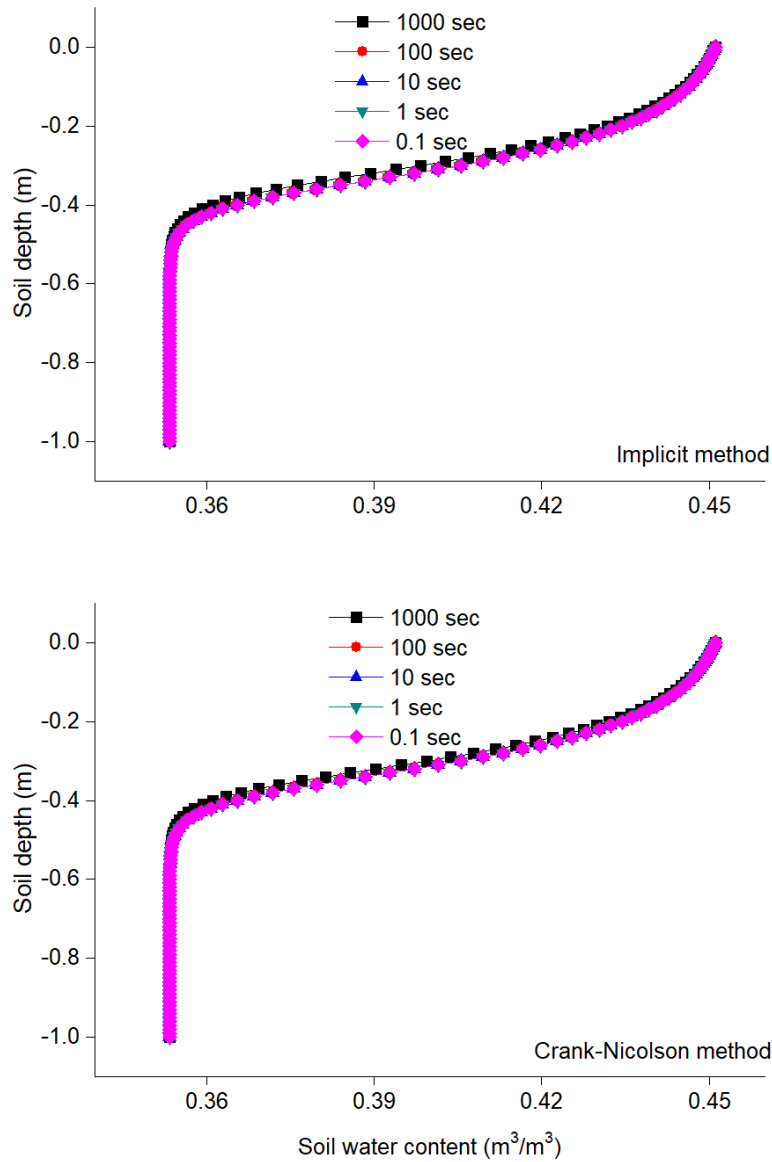
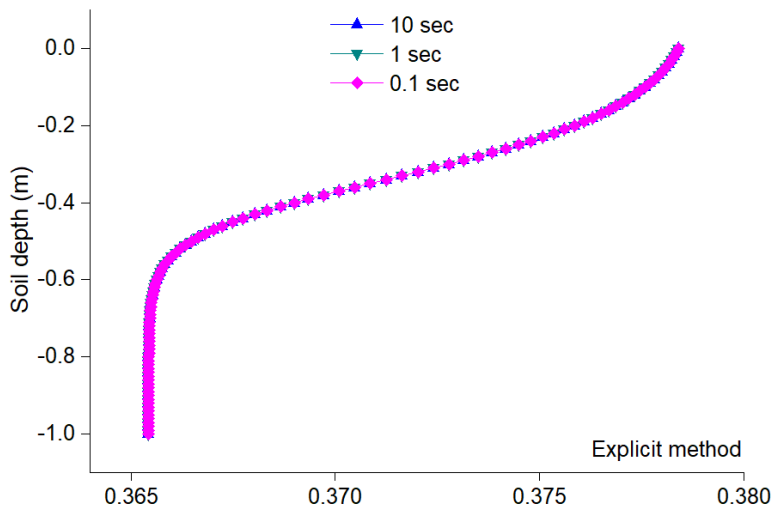


Figure 2. Soil water content obtained from simulations of the soil texture silt ($t = 24$ h). Font: Pérez et al. (2024).



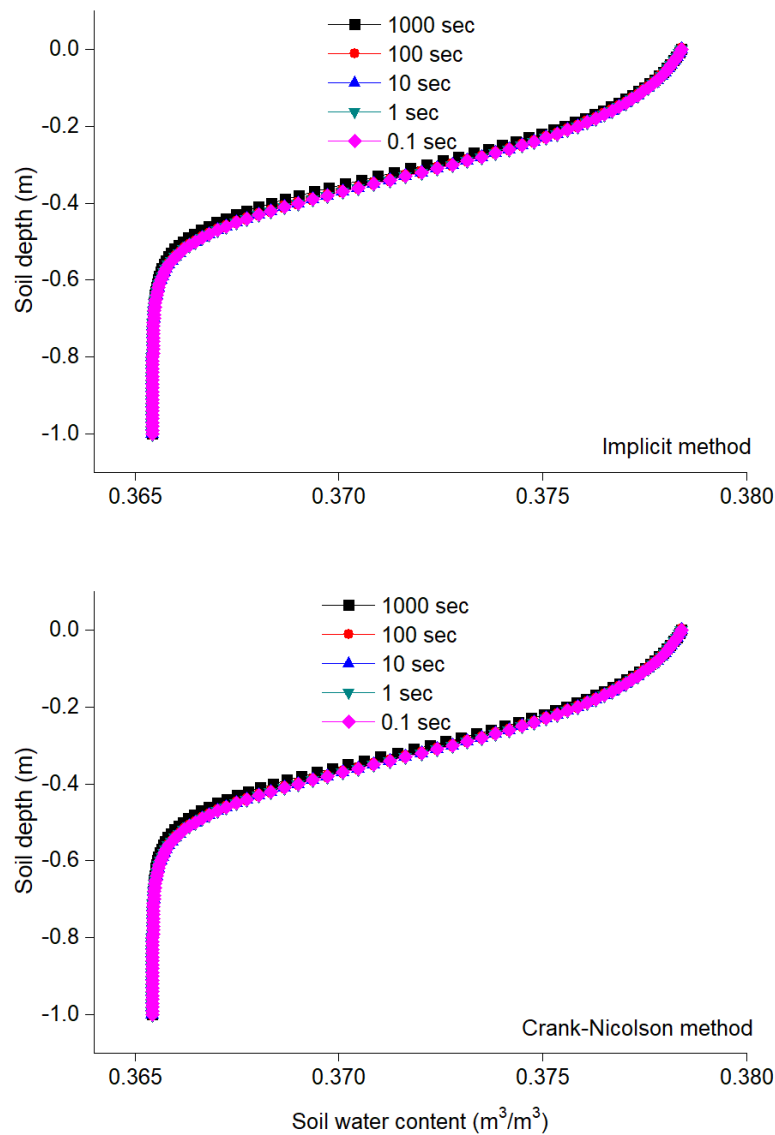


Figure 3. Soil water content obtained from simulations of the soil texture clay ($t = 24$ h). Font: Pérez et al. (2024).

Once again, the soil texture of sandy loam required the greatest requirements, 1 second using the explicit and simple implicit methods, while the Crank-Nicolson method requires 100 seconds. The soil texture silt requires a temporal discretization of 10 seconds for the explicit method, while the simple implicit and Crank-Nicolson methods require 100 seconds.

Finally, the explicit method requires a temporal discretization of 10 seconds for the clay soil texture, while the simple implicit and Crank-Nicolson methods achieve relative differences below 1% even for a dt of 1000 seconds. In summary, sandy loam had the highest discretization requirements (1 cm and 1 second), while clay had the lowest requirements (10 cm and 10 seconds).

Based on these results, all subsequent simulations will be performed using 1 cm and 1 second as discretization parameters. Figures 4 and

5 show the calculation times of the soil texture silt for each discrete spatial and time step studied. As seen in both figures, there are significant differences in the calculation times with the variation of the discretization parameters. Hence, choosing a combination of discretization parameters (dz and dt) that guarantee good accuracy and acceptable calculation times is important. It can be noted that the explicit method involves more calculation time than the implicit method. That is caused by the integral mean method used for estimating the interblocks values, which includes solving an indefinite integral of $K(h)$ over the entire range of h , to obtain a 19th-order polynomial and to evaluate it numerous times.

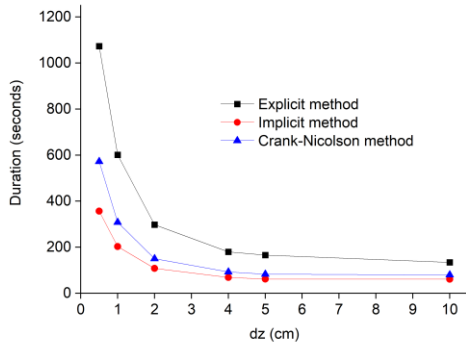


Figure 4. Calculation time of the soil texture silt for each discrete spatial step studied. Font: Pérez et al. (2024).

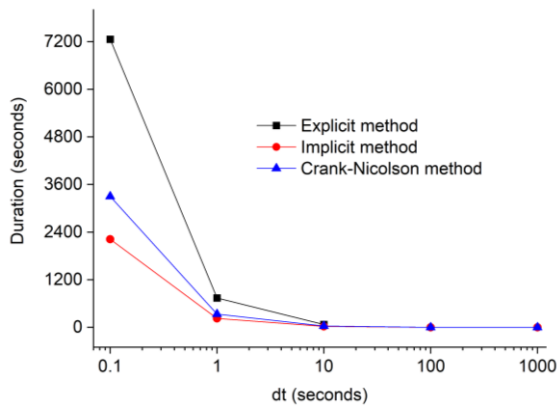


Figure 5. Calculation time of the soil texture silt for each discrete time step studied. Font: Pérez et al. (2024).

The second study included determining the soil matric potential and water content of twelve soil textures reported by (Carsel & Parrish, 1988). Those twelve soil textures cover a variety of soil types between sandy and clay. Figures 6 to 8 show the soil matric potential and water content profile with depth for the twelve soil textures using the three calculation methods. Regarding the numerical method results, three of the twelve textures showed maximum relative differences of less than 0.5%. On the other hand, the soil textures of sand, loamy sand, and sandy loam presented relative differences between the numerical methods of up to 55%.

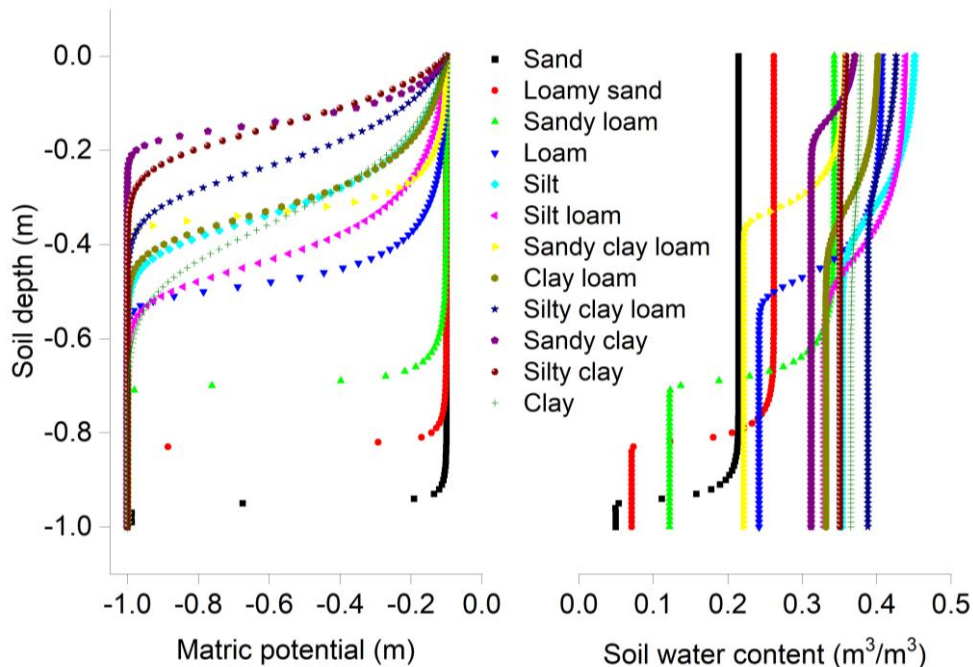


Figure 6. Matric potential and soil water content using the explicit method ($t = 24$ h). Font: Pérez et al. (2024).

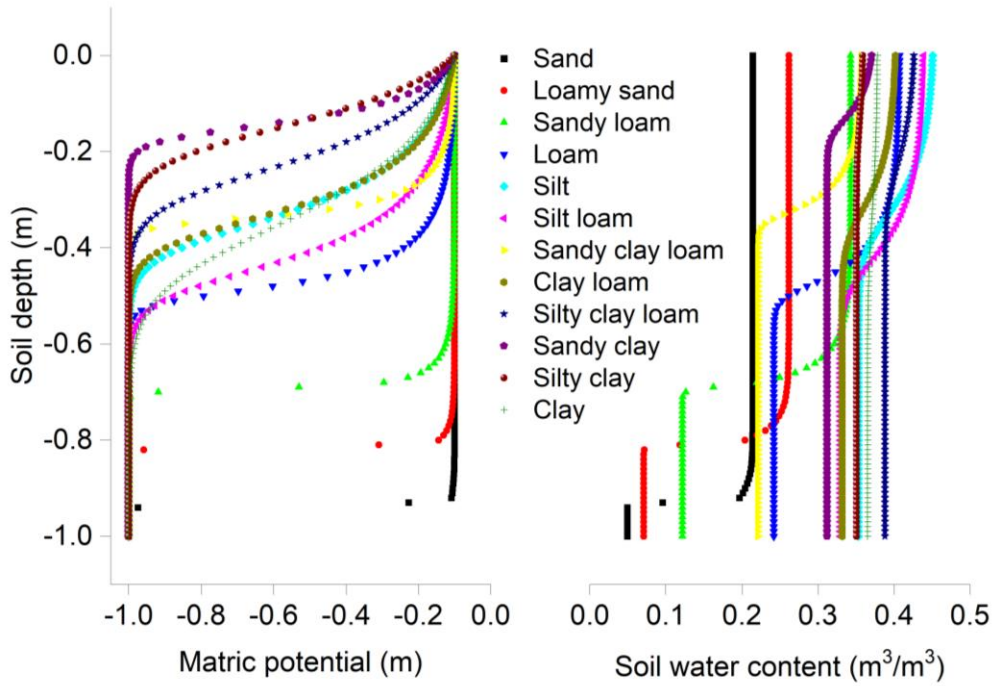


Figure 7. Matric potential and soil water content using the simple implicit method ($t = 24$ h). Font: Pérez et al. (2024).

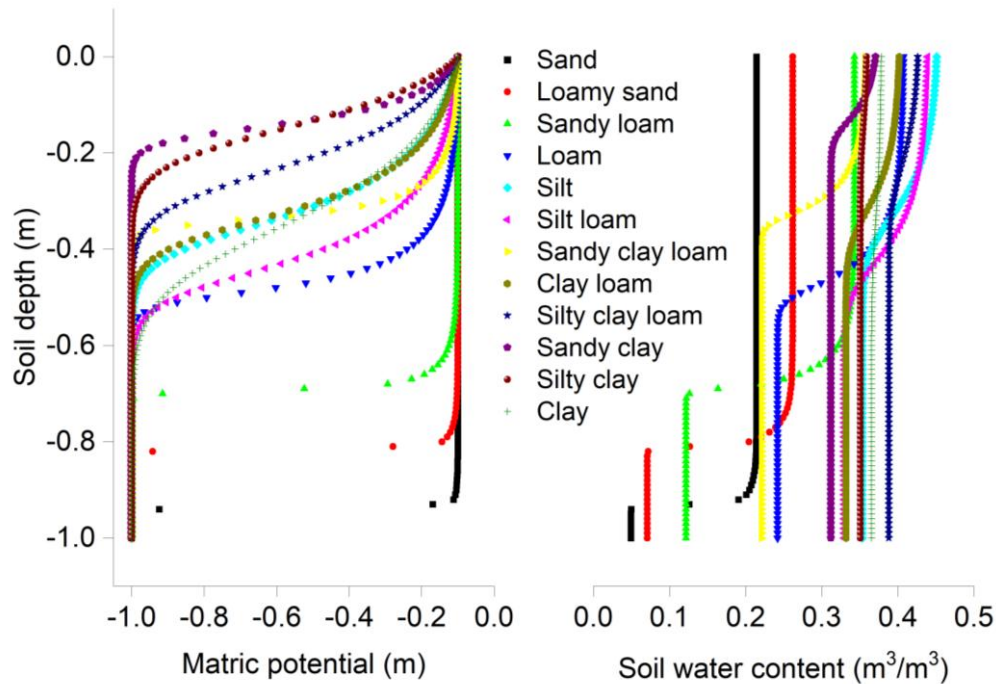


Figure 8. Matric potential and soil water content using the Crank-Nicolson method ($t = 24$ h). Font: Pérez et al. (2024).

The next step was the solution of two test cases widely used in the literature to evaluate computational models that use Richards' equation. Figure 9 shows the relation between soil water content (%) versus matric potential (kPa) of the test cases. This relation, called the moisture retention curve, allows us to characterize the composition of the soil. The comparison of the profiles of Figure 9 with those found in the scientific literature

(Fredlund & Xing, 1994) allows the identification of the soils of both test cases as sandy soil and composite soil, respectively. A similar conclusion was reported by Pedrozo et al. (2015).

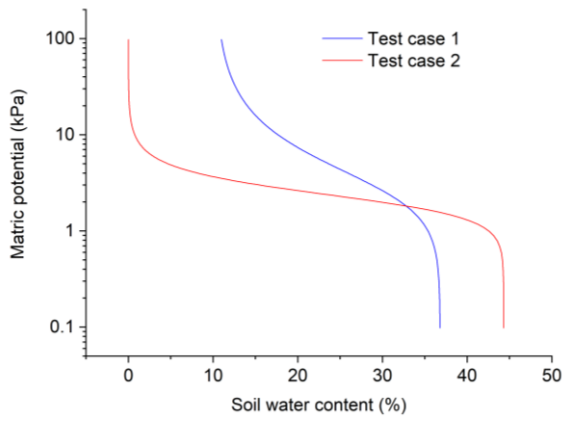


Figure 9. Moisture retention curves. Font: Pérez et al. (2024).

Figures 10 and 11 compare the results obtained with the three numerical methods (explicit, simple implicit, and Crank-Nicolson) with the results available in Celia et al. (1990) and Wendland & Pizarro (2010) for the matric potential and water content, respectively. The results obtained in this article using the three numerical methods are very similar to those reported in the literature.

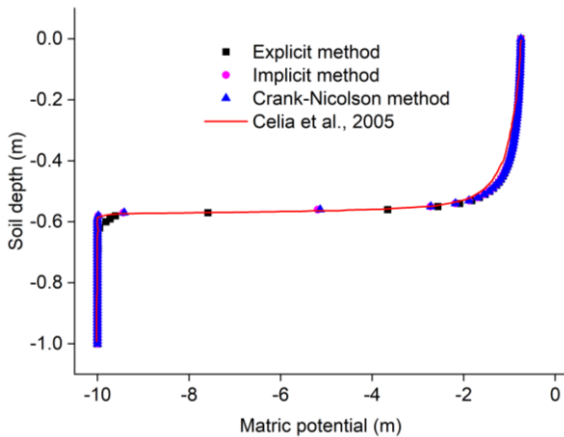


Figure 10. Comparison of the three numerical methods with the matric potential results of Celia et al. (1990). Font: Pérez et al. (2024).

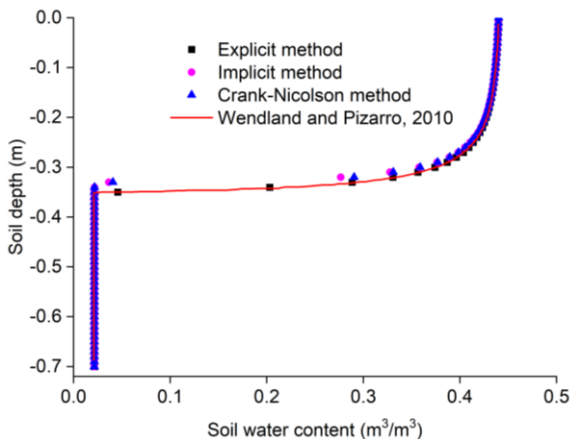


Figure 11. Comparison of the three numerical methods with the soil water content results of Wendland & Pizarro (2010). Font: Pérez et al. (2024).

Figures 12 and 13 show the relative differences between the results of each numerical method and the results available in scientific literature. As observed, maximum relative differences of 14.38% and 45.03% were obtained for the first and second test cases, respectively. In both cases, these high relative differences are in two or three nodes, specifically those nodes that correspond to the area of the wet front. In the wet front area, a large change in potential occurs in a small depth section. A possible solution for future study is using an adaptive mesh to refine this area.

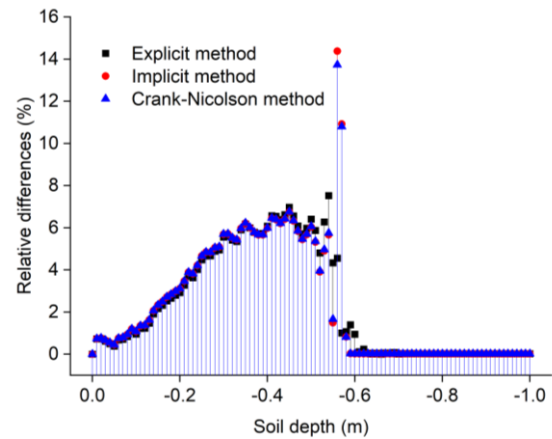


Figure 12. Relative differences of the numerical methods in comparison with the results available in the scientific literature for test case 1. Font: Pérez et al. (2024).

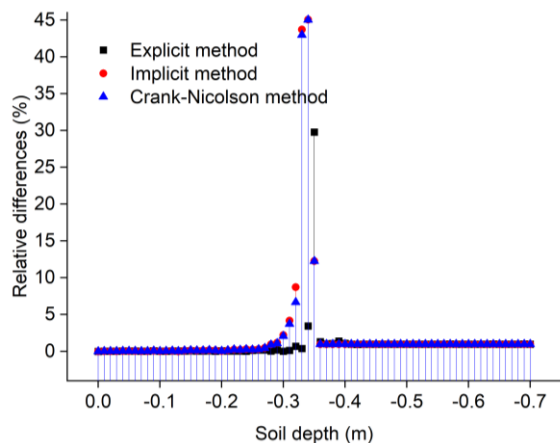


Figure 13. Relative differences of the numerical methods compared with the results available in the scientific literature for test case 2. Font: Pérez et al. (2024).

Finally, the last study conducted in this paper was focused on the simulation of soils from the semi-arid region of Brazil. The first step in

simulating these soils was to obtain the moisture retention curves for both plots, a critical factor for characterizing the composition and hydraulic behavior of the soil. Figure 14 shows the relationship between soil water content (%) and matric potential (m) for the two soils. As can be seen, the profile of the two soils is similar. However, as pointed out by Soares et al. (2020), it is evident that the representative curve for natural soil presents extreme values different from those found for cultivated soil. This significant variation reflects the impact of land use and soil management on the water retention properties of the soil. Comparing the profiles in Figure 14 with those in the scientific literature (Fredlund & Xing, 1994) reveals that both test cases can be classified as composite soils, further underscoring the complexity of soil-water interactions in these environments.

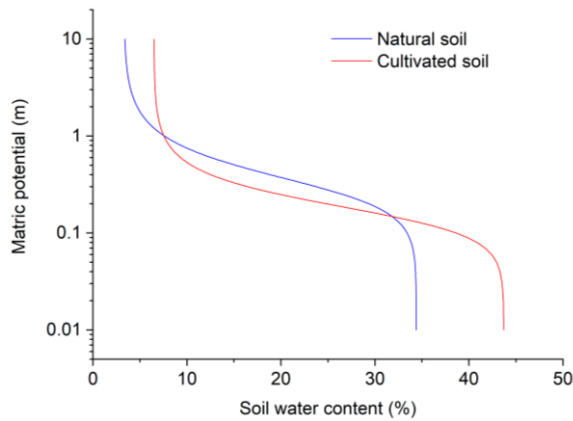


Figure 14. Moisture retention curves. Font: Pérez et al. (2024).

Figures 15 and 16 illustrate the soil matric potential and water content profiles with depth for the natural and cultivated soils, respectively. The maximum relative differences between the numerical method results were less than 0.54% for the natural soil and less than 2.75% for the cultivated soil, demonstrating the numerical model's robustness across different soil conditions. These minimal discrepancies further validate the accuracy of the proposed model in simulating soil water behavior in heterogeneous semi-arid environments. This consistency is essential for predicting soil moisture dynamics, which is critical in the sustainable management of water resources and agricultural productivity in regions facing extreme climatic variability.

The results shown in Figures 15 and 16 corroborate the findings in Figure 14, highlighting significantly higher water conduction in the cultivated soil compared to the natural soil.

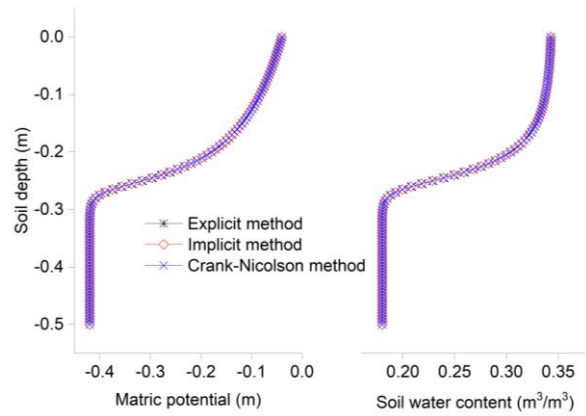


Figure 15. Soil matric potential and water content in the natural soil after 1 hour of simulation. Font: Pérez et al. (2024).

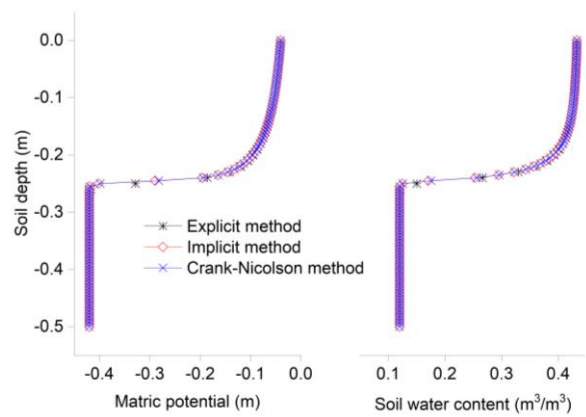


Figure 16. Soil matric potential and water content in the cultivated soil after 0.2 hours of simulation. Font: Pérez et al. (2024).

The one-order-of-magnitude difference in maximum water conduction between the two soil types is a critical finding and aligns with previous studies (Soares et al., 2020). This increased water conduction in cultivated soils, while potentially beneficial for short-term water availability, raises concerns about long-term soil health, particularly regarding erosion risks. The higher conduction speed increases the potential for soil erosion, emphasizing the urgent need for effective soil and crop management strategies in these fragile ecosystems. These results underscore the importance of adaptive land management practices to mitigate the negative impacts of intensive cultivation in semi-arid regions.

Conclusion

The computational model developed to estimate soil matric potential and water content by solving Richards' equation using finite difference methods was effective. The sensitivity analysis demonstrated that spatial steps of 1 cm and temporal steps of 1 second are sufficient to ensure accurate and discretization-independent results

across different soil textures. Sandy soils presented the greatest simulation challenges, requiring finer discretization steps.

The test cases validated the model's performance, agreeing well with previously documented results. Applications to soils from Brazil's semi-arid region revealed significant differences in water conduction profiles between natural and cultivated soils. The higher conductivity observed in cultivated soils highlights the need for adaptive management strategies to mitigate erosion risks while taking advantage of improved water availability.

These findings address the proposed objectives by evaluating the model's sensitivity and applicability to the challenging conditions of the semi-arid region. They contribute to the sustainable management of water resources and agricultural productivity under extreme climatic variability.

Acknowledgments

This research was partially supported by the Research Support Foundation of the State of Pernambuco (FACEPE), project number BFP-0146-3.09/23, and the National Council for Scientific and Technological Development (CNPq), project number 465764/2014-2 - Observatório Nacional da Dinâmica da Água e de Carbono no Bioma Caatinga (ONDACBC). The authors also acknowledge CNPq for research support, including the Junior Postdoctoral Fellowship awarded to Abel Gámez Rodríguez (Process No. 174032/2023-4) and the Productivity Fellowship granted to Antonio Celso Dantas Antonino.

References

- Althoff, D.; Rodrigues, L. N.; Silva, D. D. 2021. Addressing hydrological modeling in watersheds under land cover change with deep learning. *Advances in Water Resources*, 154, 103965. <https://doi.org/10.1016/j.advwatres.2021.103965>
- Arioli, M.; Scott, J. 2014. Chebyshev acceleration of iterative refinement. *Numerical Algorithms*, 66, (3), 591-608. <https://doi.org/10.1007/s11075-013-9750-7>
- Assouline, S.; Sela, S.; Dorman, M.; Svoray, T. 2024. Runoff generation in a semiarid environment: The role of rainstorm intra-event temporal variability and antecedent soil moisture. *Advances in Water Resources*, 188, 104715. <https://doi.org/10.1016/j.advwatres.2024.104715>
- Bittelli, M.; Campbell, G. S.; Tomei, F. 2015. *Soil Physics with Python*. In *Soil Physics with Python*. Oxford University Press. 460p. <https://doi.org/10.1093/acprof:oso/9780199683093.001.0001>
- Brito, T. R.; Lima, J. R. D. S.; Oliveira, C. L.; Souza, R. M. S.; Antonino, A. C. D.; Medeiros, E. V.; Souza, E. S.; Alves, E. M. 2020. Mudanças no Uso da Terra e Efeito nos Componentes do Balanço Hídrico no Agreste Pernambucano. *Revista Brasileira de Geografia Física*, 13, (2), 870-886. <https://doi.org/10.26848/rbgf.v13.2.p870-886>
- Carsel, R. F.; Parrish, R. S. 1988. Developing joint probability distributions of soil water retention characteristics. *Water Resources Research*, 24, (5), 755-769. <https://doi.org/10.1029/WR024i005p00755>
- Celia, M. A.; Bouloutas, E. T.; Zarba, R. L. 1990. A general mass-conservative numerical solution for the unsaturated flow equation. *Water Resources Research*, 26, (7), 1483-1496. <https://doi.org/10.1029/WR026i007p01483>
- Chapra, S. C.; Canale, R. P. 2016. *Metodos Numericos para Ingenieros*. McGraw-Hill, Seventh Edition. 864p.
- Chavarria, G.; Santos, H. P. 2012. Plant Water Relations: Absorption, Transport and Control Mechanisms. In *Advances in Selected Plant Physiology Aspects*. InTech. 29p. <https://doi.org/10.5772/33478>
- Cirilo, J. A. 2008. Políticas públicas de recursos hídricos para o semi-árido. *Estudos Avançados*, 22, (63), 61-82. <https://doi.org/10.1590/S0103-40142008000200005>
- Daneshi, A.; Brouwer, R.; Najafinejad, A.; Panahi, M.; Zarandian, A.; Maghsood, F. F. 2020. Modelling the impacts of climate and land use change on water security in a semi-arid forested watershed using InVEST. *Journal of Hydrology*, 593, 125621. <https://doi.org/10.1016/j.jhydrol.2020.125621>
- Farthing, M. W.; Ogden, F. L. 2017. Numerical Solution of Richards' Equation: A Review of Advances and Challenges. *Soil Science Society of America Journal*, 81, (6), 1257-1269. <https://doi.org/10.2136/sssaj2017.02.0058>
- Fredlund, D. G.; Xing, A. 1994. Equations for the soil-water characteristic curve. *Canadian Geotechnical Journal*, 31, (4), 521-532. <https://doi.org/10.1139/t94-061>
- Hillel, D. 1998. *Environmental soil physics*. Academic Press, First Edition. 771p.

- Leal, I. R.; Silva, J. M. C.; Tabarelli, M.; Lacher, T. E. 2005. Changing the Course of Biodiversity Conservation in the Caatinga of Northeastern Brazil. *Conservation Biology*, 19, (3), 701-706. <https://doi.org/10.1111/j.1523-1739.2005.00703.x>
- List, F.; Radu, F. A. 2016. A study on iterative methods for solving Richards' equation. *Computational Geosciences*, 20, (2), 341-353. <https://doi.org/10.1007/s10596-016-9566-3>
- Liu, F.; Qian, H.; Wang, G.; Gao, Y.; Shi, Z. 2024. New insights into the parameterization of the dry surface layer and its hydrogeochemical mechanism: An experimental study. *Advances in Water Resources*, 190, 104738. <https://doi.org/10.1016/j.advwatres.2024.104738>
- Lott, P. A.; Walker, H. F.; Woodward, C. S.; Yang, U. M. 2012. An accelerated Picard method for nonlinear systems related to variably saturated flow. *Advances in Water Resources*, 38, 92-101. <https://doi.org/10.1016/j.advwatres.2011.12.013>
- Miranda, J. H.; Duarte, S. N.; Libardi, P. L.; Folegatti, M. V. 2005. Simulação do deslocamento de potássio em colunas verticais de solo não-saturado. *Engenharia Agrícola*, 25, (3), 677-685. <https://doi.org/10.1590/S0100-69162005000300013>
- Mualem, Y. 1976. A new model for predicting the hydraulic conductivity of unsaturated porous media. *Water Resources Research*, 12, (3), 513-522. <https://doi.org/10.1029/WR012i003p00513>
- Shukla, P. R.; Skea, J.; Buendia, E. C.; Masson-Delmotte, V.; Pörtner, H. O.; Roberts, D. C.; Zhai, P.; Slade, R.; Connors, S.; Diemen, R.; Ferrat, M.; Haughey, E.; Luz, S.; Neogi, S.; Pathak, M.; Petzold, J.; Pereira, J. P.; Vyas, P.; Huntley, E.; ... Malley, J. 2019. *Climate Change and Land: An IPCC Special Report on climate change, desertification, land degradation, sustainable land management, food security, and greenhouse gas fluxes in terrestrial ecosystems*. Disponível em: <https://www.ipcc.ch/srccl>
- PBMC. 2014. *Painel Brasileiro de Mudanças Climáticas. Base científica das mudanças climáticas. Volume 1 - Primeiro Relatório de Avaliação Nacional*. Disponível em: <https://repositorio.mctic.gov.br/handle/mctic/4306>
- Pedrozo, H. A.; Rosenberger, M. R.; Schvezov, C. E. 2015. Comparison of Finite Difference Models Applied to Soil Infiltration. *RECYT*, 17, (23), 36-44.
- Pedrozo, H. A.; Rosenberger, M. R.; Schvezov, C. E. 2016. Stability analysis of the solution of the one-dimensional Richards equation by the finite difference method. *AIP Conference Proceedings*, 1738, 480008. <https://doi.org/10.1063/1.4952244>
- Rad, A. M.; Ghahraman, B.; Khalili, D.; Ghahremani, Z.; Ardakani, S. A. 2017. Integrated meteorological and hydrological drought model: A management tool for proactive water resources planning of semi-arid regions. *Advances in Water Resources*, 107, 336-353. <https://doi.org/10.1016/j.advwatres.2017.07.007>
- Richards, L. A. 1931. Capillary conduction of liquids through porous mediums. *Physics*, 1, (5), 318-333. <https://doi.org/10.1063/1.1745010>
- Schneider, R. 2003. *Explicit and Implicit Finite-Difference Methods for the Diffusion Equation in Two Dimensions*. Forschungszentrum Karlsruhe GmbH, Karlsruhe. Disponível em: <https://www.osti.gov/etdweb/biblio/20414585>
- Sishodia, R. P.; Shukla, S.; Graham, W. D.; Wani, S. P.; Jones, J. W.; Heaney, J. 2017. Current and future groundwater withdrawals: Effects, management and energy policy options for a semi-arid Indian watershed. *Advances in Water Resources*, 110, 459-475. <https://doi.org/10.1016/j.advwatres.2017.05.014>
- Soares, W. A.; Silva, S. R.; Lima, J. R. 2020. Land-use change effect on the hydro-dynamic characteristics of soil in the Brazilian semi-arid region. *Ambiente e Água - An Interdisciplinary Journal of Applied Science*, 15, (2), e2368. <https://doi.org/10.4136/ambiente-agua.2368>
- Genuchten, M. T. 1980. A Closed-form Equation for Predicting the Hydraulic Conductivity of Unsaturated Soils. *Soil Science Society of America Journal*, 44, (5), 892-898. <https://doi.org/10.2136/sssaj1980.03615995004400050002x>
- Vasconcellos, C. A.; Amorin, J. C. 2001. Numerical Simulation of Unsaturated Flow in Porous Media Using a Mass-Conservative Model. 16th Brazilian Congress of Mechanical Engineering, Uberlândia, Brasil.
- Vieira, R. M. S. P.; Tomasella, J.; Alvalá, R. C. S.; Sestini, M. F.; Affonso, A. G.; Rodriguez, D.

- A.; Barbosa, A. A.; Cunha, A. P. M. A.; Valles, G. F.; Crepani, E.; Oliveira, S. B. P.; Souza, M. S. B.; Calil, P. M.; Carvalho, M. A.; Valeriano, D. M.; Campello, F. C. B.; Santana, M. O. 2015. Identifying areas susceptible to desertification in the Brazilian northeast. *Solid Earth*, 6, (1), 347-360. <https://doi.org/10.5194/se-6-347-2015>
- Wendland, E.; Pizarro, M. L. P. 2010. Modelagem computacional do fluxo unidimensional de água em meio não saturado do solo. *Engenharia Agrícola*, 30, (3), 424-434. <https://doi.org/10.1590/S0100-69162010000300007>
- Wu, L.; He, B.; Peng, J. 2024. Analysis of Rainfall-Caused Seepage into Underlying Bedrock Slope Based on Seepage Deformation Coupling. *International Journal of Geomechanics*, 24, (5), 04024076. <https://doi.org/10.1061/IJGNAL.GMENG-9175>
- Zhu, S. R.; Wu, L. Z.; Shen, Z. H.; Huang, R. Q. 2019. An improved iteration method for the numerical solution of groundwater flow in unsaturated soils. *Computers and Geotechnics*, 114, 103113. <https://doi.org/10.1016/j.compgeo.2019.103113>